Int. J. Solids Structures Vol. 30, No. 4, pp. 579–599, 1993
Printed in Great Britain

0020–7683/93 $5.00+ .00

A CONTINUUM APPROACH TO BRITTLE AND FATIGUE DAMAGE: THEORY AND NUMERICAL PROCEDURES

M. H. J. W. PAAS
TNO Building and Construction Research—Centre for Mechanical Engineering,
P.O. Box 29, 2600AA Delft, The Netherlands

and

P. J. G. SCHREURS and W. A. M. BREKELMANS
Department of Mechanical Engineering, Eindhoven University of Technology,
Eindhoven, The Netherlands

(*Received* 18 *July* 1991; *in revised form* 24 *August* 1992)

Abstract—A unified continuum approach to brittle and fatigue damage is presented. A scalar variable is used to represent the damage state. General forms of the constitutive equations are established on a thermodynamic basis. Specific evolution laws are postulated and used to illustrate the capacity of the model. The governing equations are solved numerically. The computational effort is reduced by the application of an adaptive stepsize selection procedure for the integration of the rate equations and by uncoupling the constitutive equations. The response of a plate with an induced crack subjected to periodic loading is studied.

1. INTRODUCTION

Degradation of material properties is the result of initiation, growth and coalescence of microdefects, such as microvoids, microcracks and microcrazes. In circumstances where the defects are distributed in a statistically homogeneous manner, it is advantageous to model the mechanisms associated with material degradation within the context of continuum damage mechanics (CDM). In CDM internal state variables are introduced, which may be regarded as a continuous measure of the material degradation (Krajcinovic, 1984; Kachanov, 1986). These damage variables require the establishment of additional rate equations and criteria that indicate when the current state will change. The governing equations can be derived within a thermodynamical framework in a manner as discussed by Coleman and Gurtin (1967) and Davison and Stevens (1973). In this paper a restriction to isotropic damage is made. Then, the damage state can be represented by a scalar variable (Chaboche, 1988). In addition, only brittle failure mechanisms are considered. Brittle failure processes are characterized by the fact that damage growth is the only dissipative mechanism and that the current state does not depend on the rate at which it has been realized (Marigo, 1985). A distinction is made between brittle and fatigue damage. A unified approach is presented for both mechanisms.

The governing equations are solved numerically. This is performed by transforming the law of balance of momentum into an integral form. Then, the time domain is discretized and an incremental solution process is applied. The integral equation is discretized in space with the finite element method and solved iteratively. The internal variables are evaluated by integration of the rate equations. In situations where an explosive increase in the damage state is observed, it is efficient to uncouple the governing equations. A further reduction in computing time is achieved by using an adaptive stepsize algorithm. A test analysis is carried out to investigate the effectiveness of these time-saving procedures.

Currently much effort is spent on the modelling of macrocrack initiation and propagation by considering the crack tip as a process zone in which the damage state increases (Lemaitre, 1986). Crack growth is identified with the evolution of a completely damaged zone, without any reference to concepts taking into account the material discontinuity of the cracks. These local approaches to fracture can be applied in cases that fracture mechanics

analysis cannot cope with, thus providing a viable tool for failure analysis. The implementation in existing finite element codes is relatively straightforward as advantage can be taken of similarities with already built-in mechanisms such as plasticity. The capacity of the model is illustrated for a plate subjected to cyclic loadings.

2. GOVERNING EQUATIONS

At every instant during the deformation of a continuum, the laws of conservation of mass, momentum, angular momentum and energy must be satisfied. In addition, for every admissible process the Clausius–Duhem inequality must be satisfied. This inequality states that (Malvern, 1969)

$$-\rho(\dot{\psi}+\dot{\theta}\eta)+\boldsymbol{\sigma}:\mathbf{D}-\frac{1}{\theta}\mathbf{h}\cdot\nabla\theta \geqslant 0, \tag{1}$$

where ρ, ψ, θ, η, $\boldsymbol{\sigma}$, $\mathbf{D}$, $\mathbf{h}$ denote the mass density, the Helmholtz free energy, the absolute temperature, the specific entropy, the Cauchy stress tensor, the deformation rate tensor and the heat flow vector, respectively. The state of a body is known when for any material particle, the position vector $\mathbf{x}$ and the temperature θ are known for the whole time interval under consideration. In order to close the system of balance equations it is necessary to determine constitutive equations for η, ψ, $\boldsymbol{\sigma}$ and $\mathbf{h}$. These quantities have to satisfy a number of principles, which restrict the possible forms of the functional dependence on the independent variables (Malvern, 1969). Application of these principles yields

$$\boldsymbol{\sigma}(t)=\frac{1}{\mathbf{J}}\mathbf{F}(t)\cdot\mathbf{P}[\mathbf{E}(\tau),\theta(\tau),\mathbf{F}^{c}(\tau)\cdot\nabla\theta(\tau);\tau\leqslant t]\cdot\mathbf{F}^{c}(t), \tag{2}$$

$$\mathbf{h}(t)=\frac{1}{\mathbf{J}}\mathbf{F}(t)\cdot\mathbf{h}_{0}[\mathbf{E}(\tau),\theta(\tau),\mathbf{F}^{c}(\tau)\cdot\nabla\theta(\tau);\tau\leqslant t], \tag{3}$$

$$\psi(t),\eta(t)=\psi,\eta[\mathbf{E}(\tau),\theta(\tau),\mathbf{F}^{c}(\tau)\cdot\nabla\theta(\tau);\tau\leqslant t], \tag{4}$$

where $\mathbf{F}$, $\mathbf{P}$, $\mathbf{E}$ denote the deformation gradient tensor, the second Piola–Kirchhoff stress tensor and the Green–Lagrange strain tensor, respectively.

The inconvenient formulation of the constitutive equations in terms of functionals will be circumvented by the introduction of internal variables. Omitting thermal effects, it is assumed that the state of a body can be described completely by the instantaneous values of $\mathbf{E}$, $\dot{\mathbf{E}}$ and a set $\underline{z}$ of internal variables, which account for the influence of the past on the current values of the constitutive variables. It is proposed that the rate of the internal variables depends on the same set of variables (Coleman and Gurtin, 1967).

The Clausius–Duhem inequality (1) places further restrictions on the possible forms of the constitutive equations. For the particular set of independent variables the consequences of the restrictions with respect to the Clausius–Duhem inequality will be investigated. The rate of the free energy is given by

$$\dot{\psi}=\frac{\partial\psi}{\partial\mathbf{E}}:\dot{\mathbf{E}}+\frac{\partial\psi}{\partial\dot{\mathbf{E}}}:\ddot{\mathbf{E}}+\frac{\partial\psi^{T}}{\partial\underline{z}}\otimes\dot{\underline{z}}, \tag{5}$$

where the symbol $\otimes$ denotes a product operator. Substitution of (5) into (1) gives

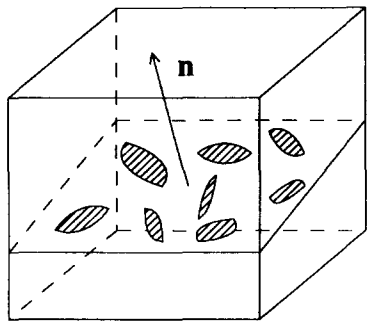

Fig. 1. Damaged volume element.

$$\left(\mathbf{P}-\rho_0\frac{\partial\psi}{\partial\mathbf{E}}\right):\dot{\mathbf{E}}-\rho_0\frac{\partial\psi}{\partial\dot{\mathbf{E}}}:\ddot{\mathbf{E}}-\rho_0\frac{\partial\psi^{\mathrm{T}}}{\partial\underline{z}}\otimes\dot{\underline{z}}\geqslant 0. \tag{6}$$

Condition (6) must hold for all possible choices of the aforementioned quantities, which leads to

$$\frac{\partial\psi}{\partial\dot{\mathbf{E}}}=\mathbf{0};\quad\left(\mathbf{P}-\rho_0\frac{\partial\psi}{\partial\mathbf{E}}\right):\dot{\mathbf{E}}-\rho_0\frac{\partial\psi^{\mathrm{T}}}{\partial\underline{z}}\otimes\dot{\underline{z}}\geqslant 0. \tag{7}$$

Inequality $(7)_2$ is always satisfied for

$$\mathbf{P}=\rho_0\frac{\partial\psi}{\partial\mathbf{E}};\quad-\rho_0\frac{\partial\psi^{\mathrm{T}}}{\partial\underline{z}}\otimes\dot{\underline{z}}\geqslant 0. \tag{8}$$

3. BRITTLE FAILURE MECHANISMS

3.1. *General theory*

Next, the modelling of brittle failure mechanisms is discussed. A distinction in the formulation of the criterion for damage evolution, is made between brittle and fatigue damage. The former develops under monotonously increasing loadings. The latter occurs for periodical loadings well below the material strength, leading to a large number of loading reversals until failure.

The damage state of materials can be defined by the existing distribution and type of microdefects (Krajcinovic, 1984; Kachanov, 1986). Consider the volume element in Fig. 1. A surface of intersection δS is identified by the normal $\mathbf{n}$. Due to the formation of microdefects in the volume element the effective load-carrying area, associated with the direction of the normal $\mathbf{n}$, is reduced from δS to δS_{e}. The damage variable associated with the direction of $\mathbf{n}$ can be defined as

$$D_{\mathrm{n}}=1-\frac{\delta S_{\mathrm{e}}}{\delta S}. \tag{9}$$

In the following, isotropic damage states are considered. This implies that D_{n} does not depend on the direction of the normal $\mathbf{n}$, such that the damage can be characterized by a scalar quantity $D=D(\mathbf{x},t)$, for which $D=D(\mathbf{x},t_0)=D_0\geqslant 0$ corresponds to the initial state and $D=D(\mathbf{x},t_{\mathrm{c}})=D_{\mathrm{c}}<1$ corresponds to complete local rupture. In brittle failure processes it is assumed that damage growth is the only dissipative mechanism. Then, the state of a body is determined by the Green–Lagrange strain tensor $\mathbf{E}$, its material time

derivative $\dot{\mathbf{E}}$ and the damage variable D. Consequently, the equations for $\mathbf{P}$, ψ and $\dot{D}$ are formulated as

$$\mathbf{P} = \mathbf{P}(\varrho); \quad \psi = \psi(\varrho); \quad \dot{D} = \dot{D}(\varrho); \quad \varrho^{\mathrm{T}} = \{\mathbf{E}, \dot{\mathbf{E}}, D\}. \tag{10}$$

Application of the Clausius–Duhem inequality (1) yields

$$\mathbf{P} = \rho_0 \frac{\partial \psi}{\partial \mathbf{E}}; \quad \psi = \psi(\mathbf{E}, D); \quad -\frac{\partial \psi}{\partial D}\dot{D} \leqslant 0. \tag{11}$$

Using the concepts of effective stress and strain equivalence (Chaboche, 1988) the constitutive equations can be written as

$$\mathbf{P} = \rho_0(1-D)\frac{\partial \psi^0}{\partial \mathbf{E}}; \quad \psi^0 = \psi(\mathbf{E}, D=0); \quad \dot{D} \geqslant 0. \tag{12}$$

In brittle mechanisms the current state does not depend upon the rate at which this state has been realized (Marigo, 1985). Mathematically this implies that the damage evolution must be positively homogeneous of degree 1 with respect to $\dot{\mathbf{E}}$

$$\dot{D}(\lambda\dot{\mathbf{E}}, \mathbf{E}, D) = \lambda\dot{D}(\dot{\mathbf{E}}, \mathbf{E}, D) \quad \forall\, \lambda \geqslant 0. \tag{13}$$

In addition to these equations, a criterion for damage growth must be established. For this purpose the existence of a closed reversible domain Ω in strain space is proposed, which contains the origin $\mathbf{E} = \mathbf{0}$ and which is bounded by the surface Γ. The damage does not grow for $\mathbf{E} \in \Omega$, but may evolve if $\mathbf{E}$ is located on the boundary Γ or outside the domain Ω. Formally the domain Ω and its boundary Γ can be expressed as

$$\Omega = \{\mathbf{E} |\, g(\mathbf{E}, \kappa) < 0\}; \quad \Gamma = \{\mathbf{E} |\, g(\mathbf{E}, \kappa) = 0\}, \tag{14}$$

where κ is a parameter that serves as a current threshold. In general its value depends on the deformation history and the material. The following set g is chosen

$$g(\mathbf{E}, \kappa) = \bar{\varepsilon}(\mathbf{E}) - \kappa \tag{15}$$

with $\bar{\varepsilon}(\mathbf{E})$ an equivalent strain measure.

3.2. *Brittle damage*

In case of brittle damage it is assumed that the boundary Γ cannot be crossed (Simo and Ju, 1987). The current state can only change if $\mathbf{E}(t) \in \Gamma$. Then, using (15), the consistency condition $\dot{g} = 0$ must be satisfied on Γ. This gives

$$\dot{\kappa} = \langle \dot{\bar{\varepsilon}} \rangle \tag{16}$$

where the McAuley brackets are defined as

$$\langle x \rangle = \begin{cases} x & \text{if } x \geqslant 0, \\ 0 & \text{if } x < 0. \end{cases} \tag{17}$$

Condition (16) describes how the boundary Γ changes. In fact it states that the damage will grow, when the equivalent strain $\bar{\varepsilon}$ reaches the current threshold κ and the strain rate is positive. If the material property κ_0 denotes the initial threshold, we must have that $\kappa \geqslant \kappa_0$. The current boundary Γ follows from integration of (16)

$$\kappa(t) = \max\,[\kappa_0, \bar{\varepsilon}(\tau)\,;\, \tau \leqslant t]. \tag{18}$$

Then, for brittle failure processes the evolution law is expressed as

$$\dot{D} = \begin{cases} 0 & \text{if } \bar{\varepsilon} < \kappa, \\ \phi(\mathbf{E}, D)\langle\dot{\bar{\varepsilon}}\rangle & \text{if } \bar{\varepsilon} = \kappa. \end{cases} \tag{19}$$

It is noted that (19) satisfies the conditions $(12)_3$ and (13). The functional dependence of ϕ on the state variables $\mathbf{E}$ and D must be established. It must provide a fairly accurate description of the underlying microstructural phenomena. For practical applications, however, the number of phenomenological constants should be kept to a minimum. A power law dependence of ϕ on the equivalent strain and damage seems to be a rational choice

$$\phi(\mathbf{E}, D) = c\bar{\varepsilon}^{d}(D_c - D)^{-e}, \tag{20}$$

where $c \geqslant 0$, d, e and D_c are material dependent parameters. Integration of the evolution law yields (provided that $d \neq -1$ and $e \neq -1$)

$$D = D_c - [(D_c - D_0)^{\alpha} - \beta(\kappa^{\gamma} - \kappa_0^{\gamma})]^{1/\alpha}, \tag{21}$$

where $\alpha = 1+e$, $\gamma = d+1$ and $\beta = c\alpha\gamma^{-1}$. Using $D_c = D(\kappa = \kappa_c)$, with κ_c the equivalent strain at complete rupture (21), becomes

$$D = D_c - (D_c - D_0)\left[\frac{\kappa_c^{\gamma} - \kappa^{\gamma}}{\kappa_c^{\gamma} - \kappa_0^{\gamma}}\right]^{1/\alpha}. \tag{22}$$

It can easily be demonstrated that for isotropic linear elastic materials the equivalent strain can be written as

$$\bar{\varepsilon} = \sqrt{\frac{2}{E}\psi^0(\mathbf{E})}, \tag{23}$$

where E is the Young's modulus. This definition does not distinguish between tensile and compressive loadings. For most brittle materials the equivalent strain should express the important part played by tension strains. A definition, which satisfies this requirement is given by

$$\bar{\varepsilon} = \sqrt{\sum_{i=1}^{3} [\langle\varepsilon_i\rangle^2 + h\langle-\varepsilon_i\rangle^2]}, \tag{24}$$

where ε_i are principal strains. In order to express that compressive strains are less harmful

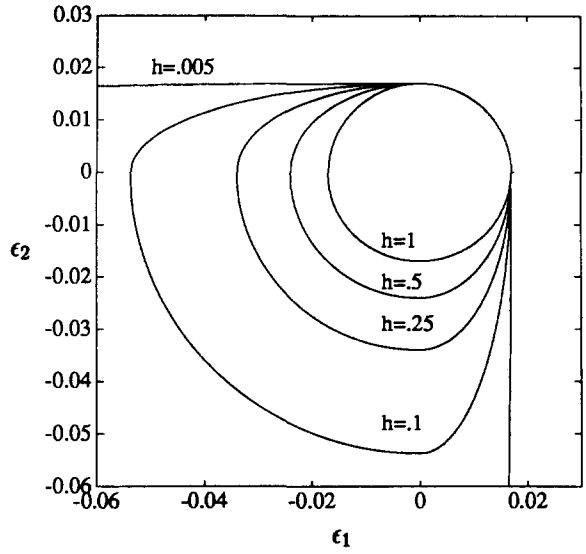

Fig. 2. Influence of h on the damage surface.

to damage growth than tensile strains, the parameter $h \in [0, 1]$ has been introduced. In Fig. 2 the influence of h on the damage surface Γ is demonstrated for $\kappa = 1.7 \cdot 10^{-2}$ and $\varepsilon_3 = 0$.

The model for brittle damage is fully specified by the stress–strain relation $(12)_1$, the definition of the equivalent strain, either (23) or (24), the relations for the current threshold (18) and damage (22). The model is illustrated with two examples. In accordance with most of the work on CDM, it is assumed that initially the material is undamaged and that the damage in the ruptured state equals one.

Concrete is known to behave as a linear elastic material that contains numerous microcracks (Bazant, 1986). The behaviour of concrete under compressive loading is investigated. From experimental observations failure in concrete is a continuous process, which initiates at low loading levels with an increasing amount of damage for increasing loading levels. The necessary model parameters are given in Table 1. The undamaged Young's modulus E_0, the threshold strain κ_0 and the failure strain κ_c were obtained from Krajcinovic and Fonseka (1981). The phenomenological constants were chosen so as to give a good fit of the experimental data presented by Krajcinovic and Fonseka (1981). In Fig. 3 the normalized model stress–strain curve for compressive loading is shown together with the experimental observations.

The same procedure was adopted to model the behaviour of Polystyrene (PS), an amorphous glassy polymer, under tensile loading. Its mechanical behaviour has been the subject of extensive investigations and in particular the role of crazing in fracture has been studied in detail (Chen *et al.*, 1981). Experimental data for PS under tension loading were obtained by Rabinowitz *et al.* (1973). These data and the fitted phenomenological constants are given in Table 1. In Fig. 4 the stress–strain curve according to the present model is

Table 1.

	Concrete	PS
E_0	27.5 GPa	3.3 GPa
κ_0	0	0
κ_c	$6 \cdot 10^{-3}$	$2.04 \cdot 10^{-2}$
α	1.25	3.25
γ	3	3
D_0	0	0
D_c	1	1

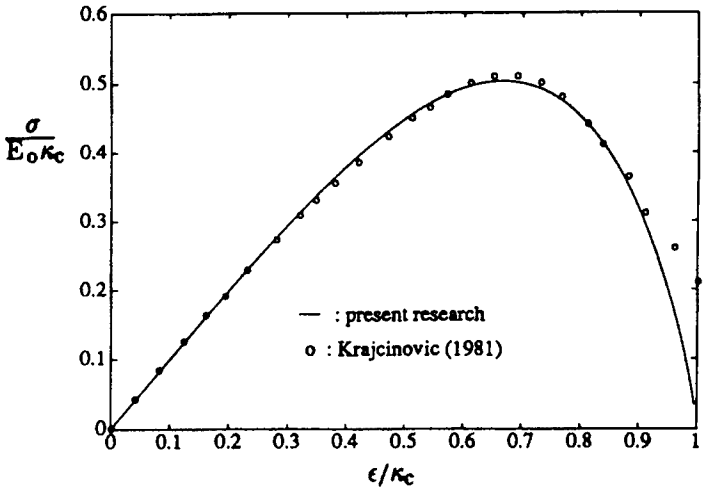

Fig. 3. Concrete under compressive loading.

shown together with the experimental data. A fair agreement between experimental and model curves in Figs 3 and 4 is revealed. These results suggest that the present damaged model is capable of describing the softening behavior of brittle materials under monotonic loadings.

3.3. *Fatigue damage*

Fatigue failure involves initiation and growth of a damaged zone, generally developing from a stress concentration site at the surface. This is followed by the initiation of a macrocrack with subsequent crack propagation until some critical crack size is reached at which catastrophic fracture occurs (Sauer and Richardson, 1980; Chaboche, 1988). In fatigue it is assumed that the boundary Γ of the domain Ω is not influenced by the deformation history and that the damage state may change if $\mathbf{E} \notin \Omega$. Then a form analogous to eqn (19) can be employed for the damage evolution law

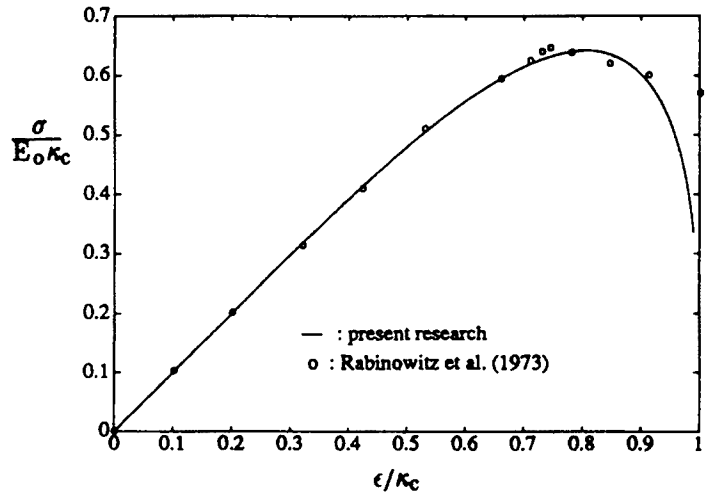

Fig. 4. PS under tensile loading.

$$\dot{D} = \begin{cases} 0 & \text{if } \bar{\varepsilon} < \kappa_0, \\ \phi(\mathbf{E}, D)\langle \dot{\bar{\varepsilon}} \rangle & \text{if } \bar{\varepsilon} \geqslant \kappa_0. \end{cases} \tag{25}$$

The evolution laws (19) and (25) differ in the sense that in fatigue the threshold $\kappa = \kappa_0$ is fixed and that the damage surface can be crossed. The functional dependence on ϕ on the equivalent strain and damage is proposed as

$$\phi = \alpha D^{\beta} \bar{\varepsilon}^{\gamma}, \tag{26}$$

where $\alpha \geqslant 0$, β, γ are material parameters. In the next section it will be demonstrated that the resulting evolution law contains some generally accepted cumulative damage laws. Substitution of (26) into (25) and integration over one period $[t_{i-1}, t_i]$ with $D(t_i) = D_i$ yields

$$\int_{D_{i-1}}^{D_i} D^{-\beta} \, \mathrm{d}D = \int_{t_{i-1}}^{t_i} \alpha H(\bar{\varepsilon} - \kappa_0) \bar{\varepsilon}^{\gamma} \langle \dot{\bar{\varepsilon}} \rangle \, \mathrm{d}\tau \equiv \delta, \tag{27}$$

where $H(\cdot)$ is the Heaviside step function.

Consider a body that is loaded in n blocks. A block is defined as a series of loading reversals between two fixed amplitudes. The kth loading block takes place for $N_{k-1} \leqslant N < N_k$ cycles with $k = 1, \ldots, n$. Assuming that the incremental damage growth per cycle is very small (27) can be replaced by a differential equation for $D(N)$ where N acts as a dimensionless time. Then the damage evolution in block k is expressed as an initial value problem

$$\frac{\mathrm{d}D}{\mathrm{d}N} = \delta_k D^{\beta}; \quad D(N = N_{k-1}) = D_{k-1}, \tag{28}$$

where D_{k-1} is the initial value at the beginning of the kth loading block. The integral δ_k must be calculated for specific loading situations. For the effective strain as sketched in Fig. 5, δ_k takes the form

$$\delta_k = \frac{\alpha}{\gamma + 1} (\bar{\varepsilon}_{m_1}^{\gamma+1} + \bar{\varepsilon}_{m_2}^{\gamma+1} - 2\kappa_0^{\gamma+1}). \tag{29}$$

3.4. *Uncoupled constitutive equations*

The constitutive equations are coupled and consequently the solution process is quite complex. In what follows an alternative solution procedure is discussed, which enables us to integrate the damage growth laws analytically. Furthermore, it will be demonstrated that the resulting expressions can be reduced to established cumulative damage laws.

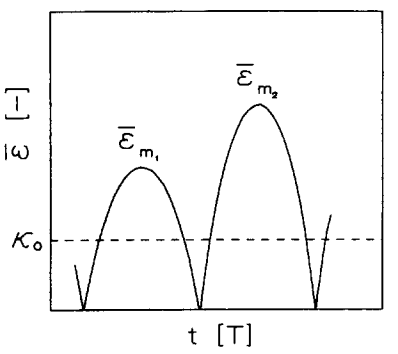

Fig. 5. Variation of $\bar{\varepsilon}$ with time.

Under the assumption that the stress tensor is not influenced by the damage, until a critical value D_c has been reached at which local rupture occurs, the concept of effective stress can be written as

$$\mathbf{P} = [1 - D_c H(D - D_c)]\hat{\mathbf{P}}. \tag{30}$$

As a result of (30) the stress–strain relation and the evolution equation have become uncoupled, implying that the local deformations are not affected by the failure process. Thus δ_k in (28) is constant during each loading block and the damage after $N_k = N_{k-1} + \Delta N_k$ cycles is

$$D_k = (\Delta N_k / \tilde{N}_{c_k} + D_{k-1}^{1-\beta})^{1/(1-\beta)}; \quad \tilde{N}_{c_k} = \frac{1}{(1-\beta)\delta_k}. \tag{31}$$

The number of cycles to failure for loading in block k is obtained by substitution of $\Delta N_k = N_{c_k}$, $D_{k-1} = D_0$ and $D_k = D_c$ into (31)

$$N_{c_k} = [D_c^{1-\beta} - D_0^{1-\beta}]\tilde{N}_{c_k}. \tag{32}$$

For loading in n blocks eqn (31) can be written as

$$D(N) = \left(\sum_{k=1}^{n} \Delta N_k / \tilde{N}_{c_k} + D_0^{1-\beta} \right)^{1/(1-\beta)}. \tag{33}$$

If the initial damage is given by $D_0 = 0$ and the critical damage is given by $D_c = 1$, (33) reduces to

$$D(N) = \left(\sum_{k=1}^{n} \Delta N_k / N_{c_k} \right)^{1/(1-\beta)}. \tag{34}$$

This cumulative damage rule is commonly referred to as the modified Palmgren–Miner damage rule (Hwang and Han, 1986). For $\beta = 0$ the so-called linear Palmgren–Miner damage rule is obtained.

4. NUMERICAL PROCEDURES

4.1. *Time discretization and linearization*

In the following the numerical solution procedure for the governing equations is discussed. Throughout the complete history of load application the balance laws must be satisfied. In the local balance equation of momentum inertial effects and body forces are omitted. According to the principle of weighted residuals the resulting equilibrium equation is equivalent to the requirement that at every instant and for all admissible weighting functions $\mathbf{w}$, the following integral equation is satisfied (Bathe, 1982)

$$\int_V \mathbf{w} \cdot (\nabla \cdot \boldsymbol{\sigma}) \, \mathrm{d}V = 0, \tag{35}$$

where V is the current volume of the body. Using integration by parts and Gauss' theorem, the so-called weak form of the principle of weighted residuals is obtained. Transformation of the weak form to the initial configuration leads to

$$\int_{V_0} (\nabla_0 \mathbf{w})^c : \mathbf{P} \cdot \mathbf{F}^c \, dV_0 = \int_{S_0} \mathbf{w} \cdot \mathbf{p}_0 \, dS_0, \tag{36}$$

where the subscript 0 denotes that the quantities are defined with respect to the initial configuration. This integral equation constitutes the basis for the finite element approximations at discrete times in the loading history.

The requirement that the weighted residuals equation is satisfied at every instant will be relaxed and replaced by the requirement that this is true for a number of discrete times $t_0, t_1, \ldots, t_n$. The time discretization results in an incremental solution process. It is supposed that the solutions up to time t_n are known and that the solution at $t_{n+1} = t_n + \Delta t_n$ is to be determined.

At time t_{n+1} the integral equation (36) is solved numerically. An iterative procedure, for determining the position vector field and its related quantities, is derived by writing all unknown quantities as the sum of an approximation of and a deviation from the exact solution. Henceforth, the real value of a quantity q at time t_{n+1} is denoted by $q(t_{n+1})$. An approximation for $q(t_{n+1})$ obtained in the ath iteration is denoted by q^a_{n+1} and the corresponding deviation is denoted by δq. The final computed value at t_{n+1} is denoted by q_{n+1}. This gives

$$\begin{aligned} &\mathbf{x}(t_{n+1}) = \mathbf{x}^a_{n+1} + \delta\mathbf{x}; \quad \mathbf{F}(t_{n+1}) = \mathbf{F}^a_{n+1} + (\nabla_0 \delta\mathbf{x})^c; \quad \underline{z}(t_{n+1}) = \underline{z}^a_{n+1} + \delta\underline{z}; \\ &\mathbf{P}(t_{n+1}) = \mathbf{P}^a_{n+1} + \delta\mathbf{P}; \quad \mathbf{p}_0(t_{n+1}) = \mathbf{p}^a_{0_{n+1}} + \delta\mathbf{p}_0. \end{aligned} \tag{37}$$

The linearized iterative change in the second Piola–Kirchhoff stress tensor $\delta\mathbf{P}$ reads

$$\delta\mathbf{P} = \left(\frac{\partial \mathbf{P}}{\partial \mathbf{E}} + \frac{\partial \mathbf{P}^T}{\partial \underline{z}} \frac{\delta \underline{z}}{\delta \mathbf{E}} \right)_{\mathbf{E}^a_{n+1}, \underline{z}^a_{n+1}} : \delta\mathbf{E} = {}^4\mathbf{C}^a_{n+1} : \delta\mathbf{E}. \tag{38}$$

Since it is impossible to give a general procedure for representing the deviations of the boundary forces in terms of $\delta\mathbf{x}$, this term is neglected in the weighted residuals formulation. Using (37) and (38) the integral equation (36) is linearized to the following expression:

$$\begin{aligned} &\int_{V_0} (\nabla_0 \mathbf{w})^c : (\mathbf{P}^a_{n+1} \cdot {}^4\mathbf{I} + {}^4\mathbf{N}^a_{n+1}) : (\nabla_0 \delta\mathbf{x}) \, dV_0 \\ &\qquad = -\int_{V_0} (\nabla_0 \mathbf{w})^c : \mathbf{P}^a_{n+1} \cdot \mathbf{F}^{a^c}_{n+1} \, dV_0 + \int_{S_0} \mathbf{w} \cdot \mathbf{p}^a_{0_{n+1}} \, dS_0, \end{aligned} \tag{39}$$

where ${}^4\mathbf{I}$ is the identity tensor of rank 4 and ${}^4\mathbf{N}$ is defined as

$${}^4\mathbf{N} : \mathbf{A} = \tfrac{1}{2}[{}^4\mathbf{C} : \{\mathbf{F}^c \cdot \mathbf{A}^c + \mathbf{A} \cdot \mathbf{F}\}] \cdot \mathbf{F}^c \quad \forall \mathbf{A}. \tag{40}$$

After having solved $\delta\mathbf{x}$ from the integral equation (39), a new approximation for the position vector field is derived. If the right-hand side of the integral equation is sufficiently small, the approximate solution is considered accurate enough. Then, the iterative process is terminated and the solution process is repeated at the next discrete time. If such is not the case the iterative process is continued.

New estimates for the internal variables must be determined by integration of the rate equations $\dot{\underline{z}} = \underline{\Xi}(\varrho(t))$, giving

$$\underline{z}(t_{n+1}) = \underline{z}(t_n) + \int_{t_n}^{t_{n+1}} \underline{F}(\varrho(\tau))\,\mathrm{d}\tau; \quad \varrho = \{\mathbf{E}, \dot{\mathbf{E}}, \underline{z}\}. \tag{41}$$

The function $\underline{F}$ is approximated by a linear polynomial between the successive times t_n and t_{n+1}

$$\underline{z}_{n+1}^{a+1} = \underline{z}_n + \tfrac{1}{2}\Delta t_n[\underline{F}_n + \underline{F}(\varrho_{n+1}^{a})]. \tag{42}$$

An initial estimate for the internal variables at t_{n+1} is obtained by substitution of the quantities at t_n in the trapezium rule (42):

$$\underline{z}_{n+1}^{1} = \underline{z}_n + \Delta t_n \underline{F}_n. \tag{43}$$

4.2. *Stepsize selection*

In order to deal efficiently with computing times, some mechanism for automatically changing the stepsize as the integration proceeds, should be employed. Intuitively, if the solution is changing very slowly, then one can use a large stepsize, whereas in regions where the solution is changing rapidly a small stepsize must be used. The stepsize must be selected before the start of the next integration step. The usual approach is to estimate the truncation error for a step and, depending on its value, adjust the current stepsize either upward or downward. The local truncation errors for $\underline{z}(t_{n+1})$ are defined by

$$\underline{L}(t_{n+1}) = \underline{z}(t_{n+1}) - \underline{z}_{n+1}. \tag{44}$$

The calculation of the truncation error $\underline{L}(t_{n+1})$ is based on approximations of the internal variables at time t_{n+1}. Since at t_n no information is available concerning the quantities at t_{n+1}, explicit integration methods should be used to calculate approximations of the internal variables. A straightforward method is to expand $\underline{z}(t)$ into a Taylor series in the neighbourhood of $\underline{z}_n$, thus

$${}^{k}\underline{z}_{n+1} = \sum_{p=0}^{k} \frac{1}{p!}\underline{z}_n^{(p)}(\Delta t_n)^p, \tag{45}$$

where $\underline{z}_n^{(p)}$ is the pth derivative with respect to time. An approximation of the local truncation error $\underline{L}_{n+1}$ of this kth order integration method is found by comparing the integration method with a higher order method, e.g. one of order $k+1$

$$\underline{L}_{n+1} = {}^{k+1}\underline{z}_{n+1} - {}^{k}\underline{z}_{n+1} = \frac{1}{(k+1)!}\underline{F}_n^{(k)}(\Delta t_n)^{k+1}. \tag{46}$$

Since the components of $\underline{z}$ require different stepsizes, the stepwise must be determined to the needs of the worst-offender equation. The most critical component of $\underline{z}$ is denoted by Z and the corresponding evolution function is denoted by T. Because Z may vary enormously in magnitude, a suitable criterion for the stepsize selection is obtained by requiring that the relative errors have a constant value e. Thus, we write

$$M_{n+1} = |{}^{k+1}Z_{n+1} - {}^{k}Z_{n+1}| = e|{}^{k+1}Z_n|, \tag{47}$$

where M_{n+1} should be considered as the desired, i.e. highest admissible, truncation error. Using (46) and (47) the stepsize is given by

$$\Delta t_n = (e(k+1)!\,|{}^{k+1}Z_n|\,|T_n^{(k)}|^{-1})^{1/(k+1)}. \tag{48}$$

The preceding equation can be cast into an equivalent form. Suppose we take the last step, i.e. $\Delta t = \Delta t_{n-1}$, and produce a local error M. Using (46) the step Δt_n, which would have given the desired truncation error M_{n+1}, is calculated as

$$\Delta t_n = \Delta t_{n-1} \left| \frac{M_{n+1}}{M} \right|^{1/(k+1)}. \tag{49}$$

If M is larger than M_{n+1}, the preceding equation indicates how much to decrease the stepsize when the present step is retried, otherwise it calculates how much the stepsize can be increased safely for the next step.

4.3. *Finite element equations*

The integral form (39) permits the solution of the unknown position vector field to be approximated by the finite element method. The weighting functions are chosen according to the Galerkin method (Bathe, 1982), which implies that the weighting functions and the position vectors are interpolated identically. As a result of this discretization eqn (39) can be written as a summation over all elements :

$$\begin{aligned}
&\sum_e \underset{\sim}{\mathbf{w}}^{e\mathrm{T}} \cdot \underline{\mathbf{K}}^e \cdot \delta \underset{\sim}{\mathbf{x}}^e = -\sum_e \underset{\sim}{\mathbf{w}}^{e\mathrm{T}} \cdot \mathbf{n}^e + \sum_e \underset{\sim}{\mathbf{w}}^{e\mathrm{T}} \cdot \mathbf{h}^e, \\
&\underline{\mathbf{K}}^e = \int_{V_0^e} (\nabla_0 \underset{\sim}{\phi}) \cdot (\mathbf{P}^a_{n+1} \cdot {}^4\mathbf{I} + {}^4\mathbf{N}^a_{n+1}) \cdot (\nabla_0 \underset{\sim}{\phi}^{\mathrm{T}})\, \mathrm{d}V_0, \\
&\underset{\sim}{\mathbf{n}}^e = \int_{V_0^e} (\nabla_0 \underset{\sim}{\phi}) \cdot \mathbf{P}^a_{n+1} \cdot \mathbf{F}^{ac}_{n+1}\, \mathrm{d}V_0, \\
&\underset{\sim}{\mathbf{h}}^e = \int_{S_0^e} \underset{\sim}{\phi}\, \mathbf{p}^a_{0_{n+1}}\, \mathrm{d}S_0,
\end{aligned} \tag{50}$$

where $\delta \underset{\sim}{\mathbf{x}}^e$ and $\underset{\sim}{\mathbf{w}}^e$ are columns containing the iterative changes in the nodal point position vectors and weighting functions of element e, and $\underset{\sim}{\phi}$ is the corresponding column of interpolation functions ; $\underline{\mathbf{K}}^e$ denotes the element stiffness matrix and the columns $\underset{\sim}{\mathbf{n}}^e$ and $\underset{\sim}{\mathbf{h}}^e$ store the internal and external nodal forces, respectively. Assemblage of all element stiffness matrices and internal and external element forces leads to a linear set of equations for the iterative changes in the nodal point position vectors

$$\underline{\mathbf{K}} \cdot \delta \underset{\sim}{\mathbf{x}} = \underset{\sim}{\mathbf{r}}. \tag{51}$$

In each iteration a residual load vector $\underset{\sim}{\mathbf{r}}$ and the stiffness matrix $\underline{\mathbf{K}}$ are calculated. The iterative changes in the nodal point position vectors are obtained by solving (51). Then, new approximations of the quantities that depend upon the nodal point position vectors are calculated. Subsequently, new approximations for the internal variables are determined by numerical integration of the evolution equations. The iterative process is continued until the residual load vector or the iterative changes in the position vectors are sufficiently small. For the next applications a four-node isoparametric element was chosen for the evaluation of the element stiffness matrix and the element nodal forces.

4.4. *Test analysis*

The performance of the algorithm for the numerical integration of the evolution equations is checked. The case to be considered involves fatigue loading of a plate. It is assumed that the stress–strain relation is given by (12).

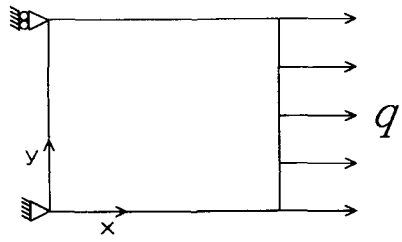

Fig. 6. Plate subjected to uniaxial loading.

Consider a plate of dimensions $25 * 25 * 0.5$ $[L^3]$, which is loaded at the free edge $x = 25$ $[L]$ by a distributed cyclic force q (Fig. 6). The stress state in the plate is homogeneous and uniaxial. For an isotropic linear elastic material the stress–strain relation becomes

$$\begin{bmatrix} \hat{P}_{11} \\ 0 \\ 0 \end{bmatrix} = \frac{E}{(1+\nu)(1-2\nu)} \begin{bmatrix} 1-\nu & \nu & \nu \\ \nu & 1-\nu & \nu \\ \nu & \nu & 1-\nu \end{bmatrix} \begin{bmatrix} E_{11} \\ E_{22} \\ E_{33} \end{bmatrix}. \tag{52}$$

The external loading will cause the plate to deteriorate. For fixed loading amplitudes 0 and q_m, the equivalent strain in one cycle will vary between 0 and $\bar{\varepsilon}_m$. It is assumed that the deformation in thickness direction does not influence defect growth. Using (24) and (52) the equivalent strain can be written as

$$\bar{\varepsilon} = \sqrt{1+h\nu^2}\, E_{11}. \tag{53}$$

The damage evolution law is given by [see eqns (28) and (29)]

$$\frac{\mathrm{d}D}{\mathrm{d}N} = \frac{\alpha}{\gamma+1}(\bar{\varepsilon}_m^{\gamma+1} - \kappa_0^{\gamma+1}) D^{\beta} \; ; \quad D(N=0) = D_0. \tag{54}$$

As the displacement field is dependent upon the current damage state, the governing equations must be solved numerically. However, when the elastic and dissipative mechanisms are uncoupled according to (30) an analytical solution can be established [cf. eqn (33) for $n = 1$]. The model parameters are given in Table 2. The calculations were accomplished for loadings ranging from 0 to $q_m = 17.2$ $[F \cdot L^{-1}]$. The stepsize has been computed according to (49).

In Fig. 7 the damage is depicted as a function of the number of cycles for different relative truncation errors e. For each e the numerical solutions for the coupled and uncoupled equations are shown together with the analytical solution for the uncoupled equations. The small deviations between the solutions for the coupled and uncoupled equations indicate that the application of the uncoupled equations should be favoured with regard to computing times. This is illustrated further in Table 3, where the computing times for both solution methods are given for different relative errors e. The computing times are scaled to the smallest value, which is obtained in the uncoupled situation with $e = 0.1$. For a relative error $e = 0.01$ the numerical integration shows greatest accuracy, but with associated larger computational effort.

Table 2. Material data

$E = 3 \cdot 10^3$ $[FL^{-2}]$	$\alpha = 5.35 \cdot 10^5$
$\nu = 0.25$	$\beta = 1.4$
$h = 0.2$	$\gamma = 2.6$
$D_0 = 2.4 \cdot 10^{-5}$	$\kappa_0 = 0$

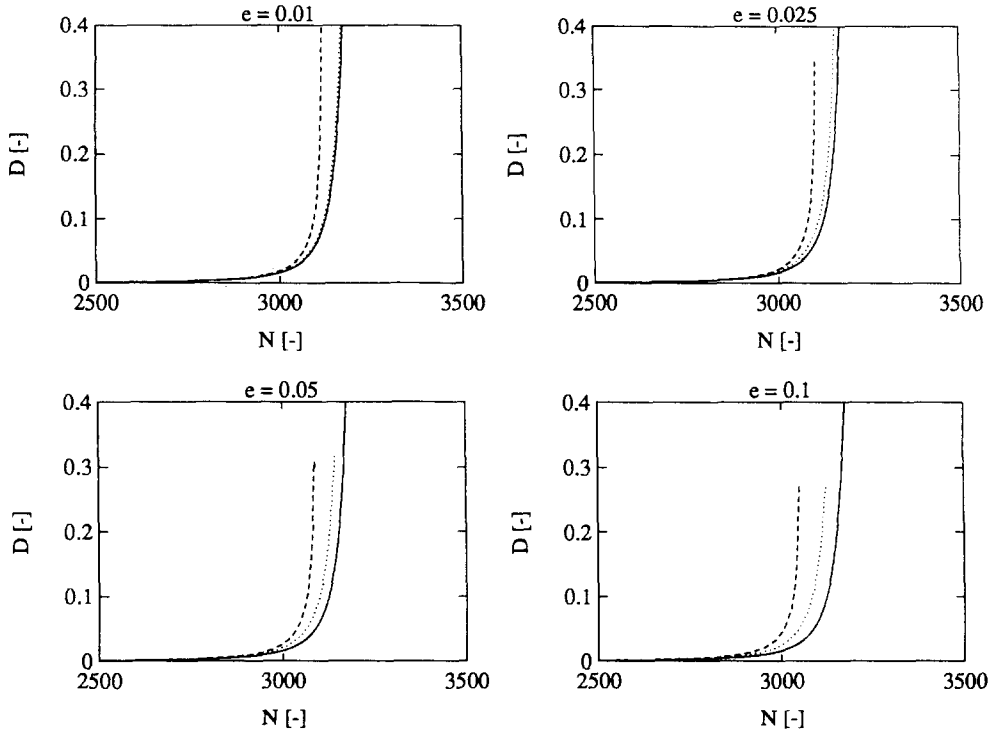

Fig. 7. D as a function of N for different relative errors e; --- coupled equation, ···· uncoupled equation, —— analytical solution.

The stepsize selection procedure is illustrated for $e = 0.025$. In Fig. 8 the damage evolution is shown as a function of the number of cycles. The instants, at which the incremental analysis was carried out, are marked. In Fig. 9 the equivalent strain is depicted as a function of the number of cycles. For the uncoupled equations the equivalent strain has a constant value until a critical damage level is reached. For the coupled equations the equivalent strain is a continuously increasing function that follows the damage evolution. In Fig. 10 the stepsize (in cycles) is shown as a function of the number of steps. The stepsize selection procedure performs very well, computing relatively large steps when the damage is changing slowly and continuously decreasing steps as the damage increases. The deviations between the stepsize selections for the coupled and uncoupled equations result from a different first derivative in (48). Hence, a substantial reduction in computing time is achieved with the adaptive stepsize control.

It is remarked that conclusions drawn from the uniaxial stress state will also hold for multi-axial stress states. A multi-axial stress state will merely result in a different damage equivalent strain. For example, in the case of a biaxial loading with the same kinematic boundary conditions, but with $P_{11} = P_{22} = P$, the equivalent strain will become $\bar{\varepsilon} = \sqrt{2}E_{11}$.

5. CRACK GROWTH IN PLATE

The fatigue damage model is used to predict crack growth with a local approach to fracture. Here a crack is represented as a zone of critically damaged elements (Lemaitre,

Table 3. Relative CPU times

e	Coupled	Uncoupled
0.01	36.4	1.7
0.025	27.1	1.3
0.05	21.8	1.1
0.1	18	1

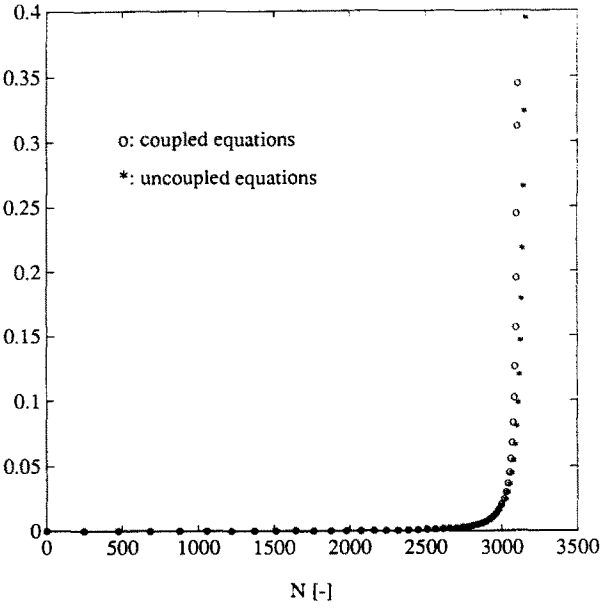

Fig. 8. D as a function of N ($e = 0.025$).

1986). To characterize the initial damage, each element in the mesh is divided into four subareas S_i, $i \in \{1, 2, 3, 4\}$ (Fig. 11). The subareas are the Gauss point influence zones, which comprise the points where the constitutive equations are evaluated. Since materials typically contain flaws of unknown dimensions and positions, the initial damage should be considered as a random quantity. Paas *et al.* (1990) presented a model for determining the statistics of the initial damage. In this model the random damage is associated with the elementary cell (EC) surface. The elementary cell surface A_{ec} is a material property. Its value can be

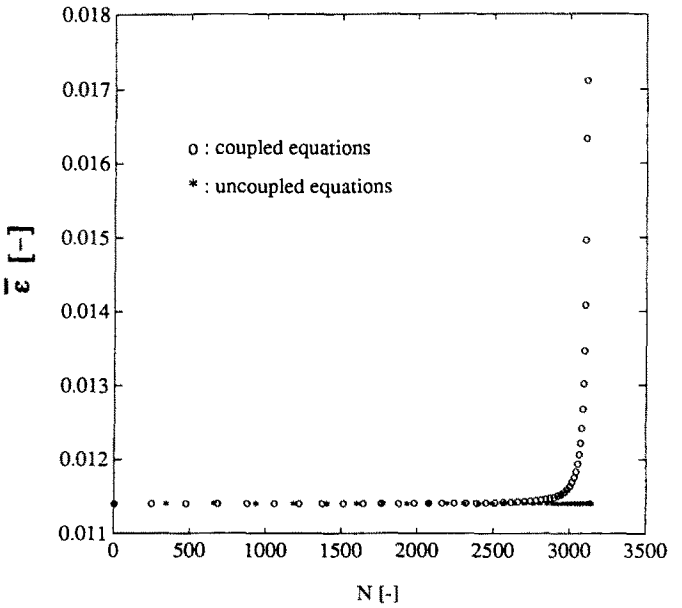

Fig. 9. $\bar{\varepsilon}$ as a function of N ($e = 0.025$).

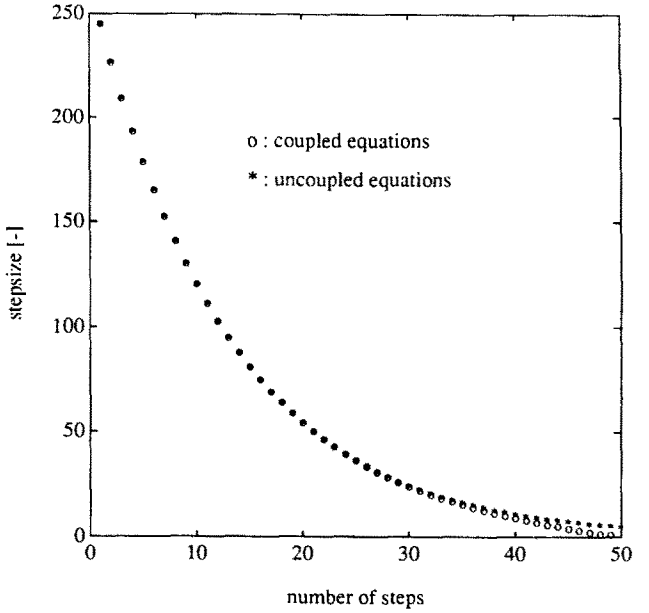

Fig. 10. Stepsize vs number of steps ($e = 0.025$).

determined by fitting a model probability distribution function of the maximum damage in a test specimen to the corresponding experimental probability distribution function. The resulting best-fit parameters are the elementary cell surface area and the associated mean maximum damage. The subarea S_i consists of $k_i = S_i/A_{ec}$ elementary cells. Due to the finite element discretization the stress state in S_i is almost homogeneous. Then first failure occurs in the EC with the largest initial damage. It is assumed that this event marks the complete failure of a subarea. Thus the strength of the weakest EC is the limiting factor in the reliability of the subarea S_i. Under the assumption that the probability density function (PDF) of the damage in an EC is distributed exponentially, the PDF of the maximum initial damage in S_i is given by (Paas, 1990; Paas *et al.*, 1990).

$$f_D(D) = k_i\lambda \exp(-\lambda D)[1-\exp(-\lambda D)]^{k_i-1}; \quad k_i = S_i/A_{ec}, \tag{55}$$

where $1/\lambda$ is the mean damage in an EC.

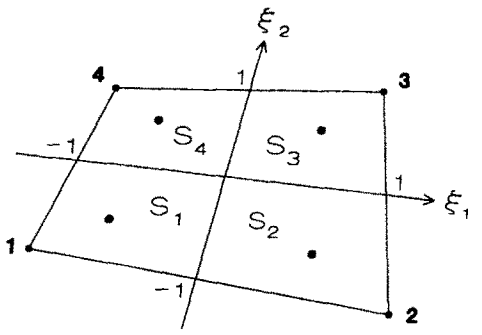

Fig. 11. plane stress element divided into four subareas.

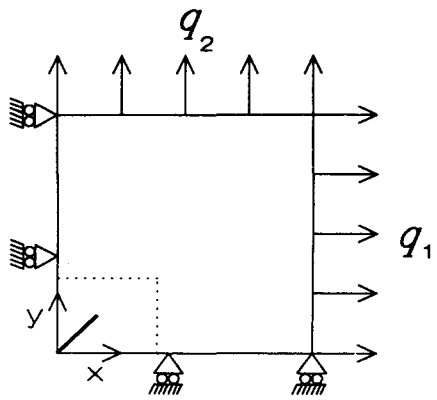

Fig. 12. Plate with an induced crack.

Consider the plate of dimensions $130 * 130 * 0.1$ $[L^3]$ in Fig. 12. A crack of length $20\sqrt{2}$ $[L]$ is induced at the origin at angle of 45°. The plate is loaded by a cyclic force (q_1, q_2), which varies between $(0, 0)$ and (q_1, q_2). The corresponding finite element mesh is shown in Fig. 13. As a result of the randomness in the initial damage state failure is a stochastic process and simulation techniques must be utilized. As our main concern is the prediction of crack patterns, only one calculation has been carried out for each load case. In this calculation the initial damage in the elements is given by the expected values of the PDF (55). As a consequence large values for the initial damage state will be contributed to large subareas. The analysis has been performed for the uncoupled constitutive equations using a relative error of $e = 0.025$. The material data are given in Table 4.

Table 4. Material data for crack propagation

$E = 3 \cdot 10^3$ $[F \cdot L^{-2}]$	$D_c = 0.995$
$\nu = 0.25$	$\kappa_0 = 0$
$\alpha = 1.93 \cdot 10^6$	$\kappa_c = 4 \cdot 10^{-2}$
$\beta = 1.4$	$\lambda = 9.6 \cdot 10^4$
$\gamma = 2.6$	$A_{ec} = 0.3$ $[L^2]$
$h = 0.2$	

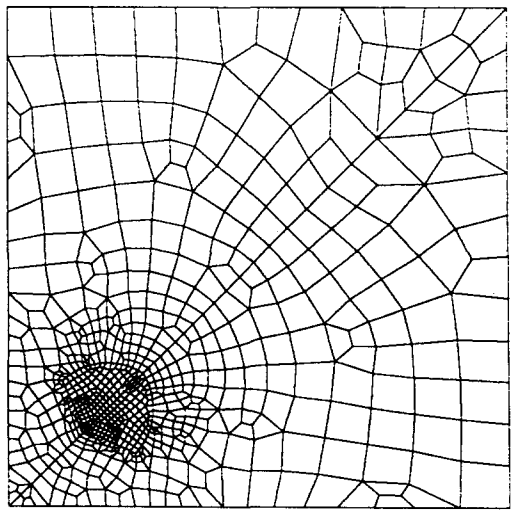

Fig. 13. Finite element discretization of plate.

Crack initiation and growth are determined for different types of loading. The loading is characterized by the ratio of the force amplitudes $\vartheta = q_2/q_1$. The amplitude q_1 is kept fixed at 0.74 $[F \cdot L^{-1}]$. Three situations are examined:

(1) $\vartheta = 1$

As the loading and the boundary conditions are symmetrical, a crack will develop from the induced crack tip and proceed along the axis of symmetry. In Fig. 14(a) the crack pattern is shown for $N = 6.65 \cdot 10^3$ cycles. The corresponding von Mises stresses are shown as well; dark regions mark the position of the current crack tip.

(2) $\vartheta = 0$

Due to the non-symmetrical stress-state a crack initiates at the induced crack tip and propagates straight to the left. In Fig. 14(b) the crack pattern and the corresponding von Mises stresses are shown for $N = 1.4 \cdot 10^4$ cycles.

(3) $\vartheta = 0.5$

In this case a combination of the failure processes in (1) and (2) is obtained. In Fig. 14(c) the crack and the corresponding von Mises stresses are depicted for $N = 1.4 \cdot 10^4$ cycles. In contrast with the cracks that have developed for $\vartheta = 1$ and $\vartheta = 0$, the crack for $\vartheta = 0.5$ is not straight. Until some transition phase is reached the crack proceeds identically to the crack for loading in x-direction ($\vartheta = 0$). Thereafter the crack proceeds in accordance with the crack for equal loading amplitudes ($\vartheta = 1$). This is a self-repeating process, as a result of which the crack will zigzag through the plate.

6. DISCUSSION

In this paper a continuum damage approach was adopted to describe brittle failure mechanisms. Brittle failure processes require the establishment of the stress–strain relation and the damage evolution equation together with a criterion for damage growth. A scalar variable was used to represent the damage state. The stress–strain relation was based on the concepts of effective stress and strain equivalence. A distinction, which is based on the formulation of the damage criterion, was made between brittle and fatigue damage. For brittle damage the damage surface may grow under given loading conditions, but for fatigue damage the surface is invariable. The equivalent strain accounts for the fact that tensile and compressive loadings contribute differently to the failure process. The mathematical representation of the evolution laws was based on a power law dependence on equivalent strain and damage. The mechanical behaviour of concrete and polystyrene under uni-axial loading showed good agreement with experimental observations. The model developed for fatigue loading has been shown to yield some generally accepted cumulative damage models.

The resulting equations were solved numerically. A substantial reduction of computing time was achieved by employing an adaptive stepsize algorithm. A further reduction in computing time was achieved by uncoupling the stress–strain relation and the damage evolution equation. For failure mechanisms, which show an explosive increase in the damage state, the uncoupling is to be favoured.

A local approach to fracture was used to predict both crack initiation and propagation by representing the crack as a zone of completely damaged elements. As our main concern was directed towards the qualitative prediction of the crack pattern, only one calculation was carried out by attributing the expected values of the initial damage distribution to the Gauss points in the mesh. Crack propagation in a plate with an induced crack was studied for three distinct loadings. Although no reference can be made to other studies, the results are qualified as promising. Future work will be devoted to the statistics of the damage variable and its effects on failure prediction. These issues are closely related to the reduction of the mesh sensitivity, which can be obtained using the concept of the elementary cell as a characteristic scale in the mesh.

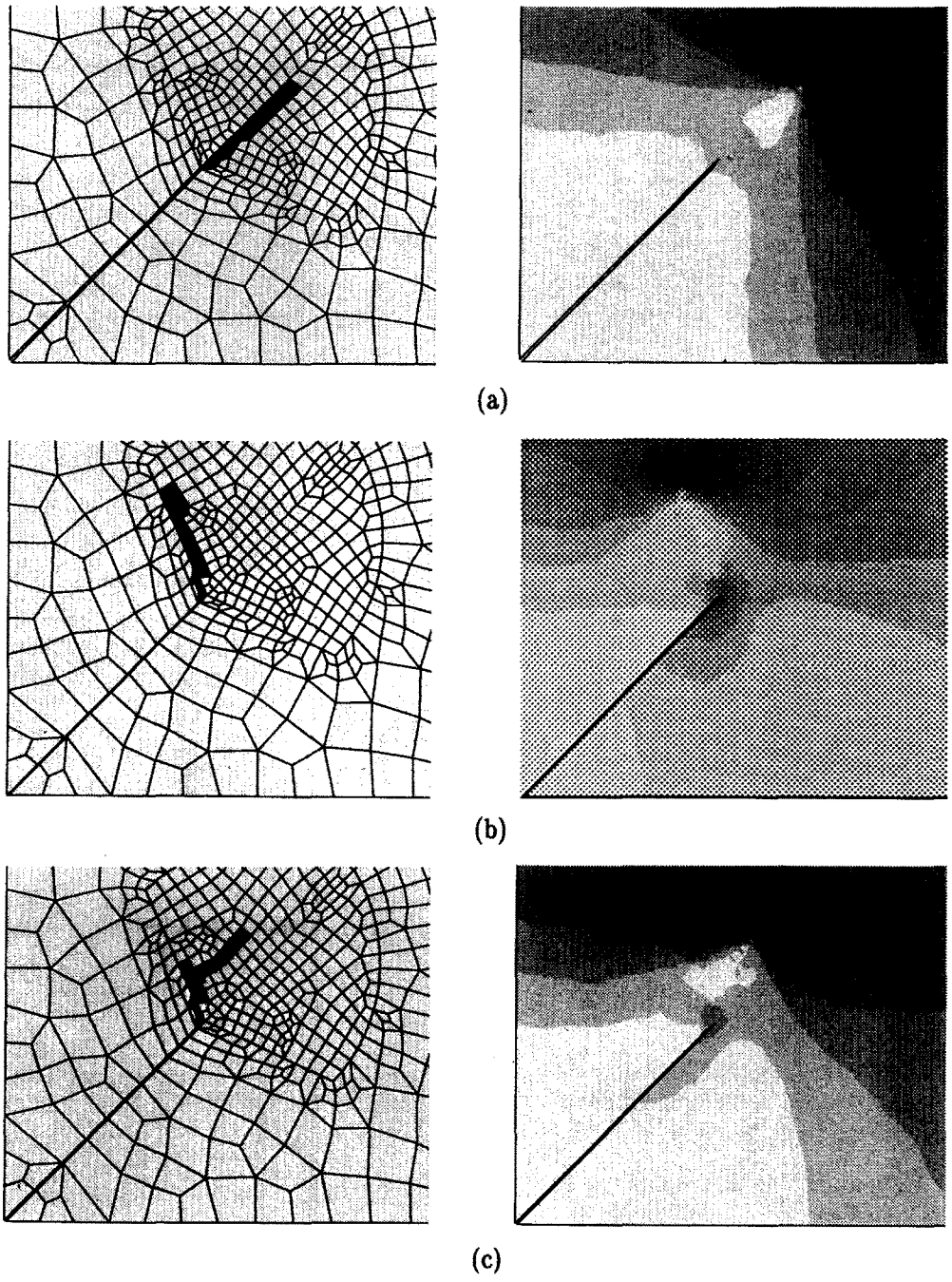

Fig. 14. Crack patterns and corresponding von Mises stresses for (a) $\vartheta = 1$, (b) $\vartheta = 0$ and (c) $\vartheta = 0.5$.

REFERENCES

Bathe, K. J. (1982). *Finite Element Procedures in Engineering Analysis*. Prentice-Hall, Englewood Cliffs.

Bazant, Z. P. (1986). Mechanics of distributed cracking. *Appl. Mech. Rev.* **39,** 675–705.

Chaboche, J. L. (1988). Continuum damage mechanics, parts 1 and 2. *J. Appl. Mech.* **55,** 59–72.

Chen, C. C., Chheda, N. and Sauer, J. A. (1981). Craze and fatigue resistance of glassy polymers. *J. Macromol. Sci—Phys.* **B19,** 565–588.

Coleman, B. D. and Gurtin, M. E. (1967). Thermodynamics with internal state variables. *J. Chem. Phys.* **47,** 597–613.

Davison, L. and Stevens, A. L. (1973). Thermomechanical constitution of spalling elastic bodies. *J. Appl. Phys.* **44,** 668–674.

Hwang, W. and Han, K. S. (1986). Cumulative damage models and multi stress fatigue life prediction. *J. Composite Mater.* **20,** 125–153.

Kachanov, L. M. (1986). *Introduction to Continuum Damage Mechanics*. Martinus Nijhoff, Dordrecht.

Krajcinovic, D. (1984). Continuum damage mechanics. *Appl. Mech. Rev.* **37,** 1–6.

Krajcinovic, D. and Fonseka, G. U. (1981). The continuous damage theory of brittle materials. Parts 1 and 2. *J. Appl. Mech.* **48,** 809–824.

Lemaitre, J. (1986). Local approach of fracture. *Engng Fract. Mech.* **25,** 523–537.

Malvern, L. E. (1969). *Introduction to the Mechanics of a Continuous Medium*. Prentice-Hall, Englewood Cliffs.

Marigo, J. J. (1985). Modelling of brittle and fatigue damage for elastic material by growth of microvoids. *Engng Fract. Mech.* **21,** 861–874.

Paas, M. H. J. W. (1990). Continuum damage mechanics with an application to fatigue. Ph.D. thesis, Eindhoven University of Technology, Eindhoven, The Netherlands.

Paas, M. H. J. W., Oomens, C. W. J., Schreurs, P. J. G. and Janssen, J. D. (1990). The mechanical behaviour of continuous media with stochastic damage. *Engng Fract. Mech.* **36,** 255–266.

Rabinowitz, S., Krause, A. R. and Beardmore, P. (1973). Failure of polystyrene in tensile and cyclic deformation. *J. Mater. Sci.* **8,** 11–22.

Sauer, J. A. and Richardson, G. C. (1980). Fatigue of polymers. *Int. J. Fract.* **16,** 499–532.

Simo, J. C. and Ju, J. W. (1987). Strain- and stress-based continuum damage models—I. Formulation. *Int. J. Solids Structures* **23,** 821–840.